Spin-flop transition in the easy-plane antiferromagnet nickel oxide

F. L. A. Machado,[1] P. R. T. Ribeiro,[1] J. Holanda,[1] R. L. Rodríguez-Suárez,[2] A. Azevedo,[1] and S. M. Rezende[1,*]

[1]*Departamento de Física, Universidade Federal de Pernambuco, 50670-901, Recife, Pernambuco, Brazil*
[2]*Facultad de Física, Pontificia Universidad Católica de Chile, Casilla 306, Santiago, Chile*

NiO is a room-temperature antiferromagnetic (AF) insulator with important applications in AF spintronics. Although it is considered a prototypical AF material with a simple magnetic structure with two sublattice spins aligned in easy planes and having small in-plane magnetic anisotropy, its critical behavior has not been studied in detail. Here we present an experimental investigation of the critical magnetic field for the transition from the AF to the spin-flop (SF) phase obtained with magnetization and susceptibility measurements. The measured temperature dependence of the AF-SF critical field can be quite well explained by the instability of the low-lying magnon mode with energy renormalized by four-magnon interactions.

I. INTRODUCTION

The recent emergence of antiferromagnetic spintronics has renewed the interest in antiferromagnetic (AF) materials [1–11]. These materials play an essential role in the most important spintronic device, namely spin-valve reading heads employed in hard-disk drives [12]. However, they only have the passive role of pinning the magnetization of a reference magnetic layer by means of the interfacial exchange bias [13,14]. Recent discoveries of the spin-Hall effect in metallic AFs [15–18], of the spin-Seebeck and spin-Nernst effects [19–23], and spin transport [24–30] in several AFs have contributed to draw attention to this class of materials. Furthermore, it has been realized that the unique properties of AF materials can be exploited in spintronic devices with new functionalities, such as in magnetic storage elements that are very robust against magnetic field perturbations [10,31,32] and with much faster dynamics than in ferromagnets [33].

NiO is considered a prototypical room temperature antiferromagnetic insulator because of its simple structure and spin interactions. Its magnetic structure and spin interactions were revealed several decades ago [34,35]. In the paramagnetic phase NiO has the face-centered-cubic structure of sodium chloride. Below the Néel temperature $T_N \approx 523$ K, the Ni^{2+} spins are ordered ferromagnetically in {111} planes, lying along $\langle 11\bar{2} \rangle$ axes, with adjacent planes oppositely magnetized due to a superexchange AF interaction. This material has been extensively used in experimental investigations of many phenomena, such as exchange bias [12–14,36,37], inelastic light scattering [38–40], and magnetic response with THz frequencies [41–43]. More recently it has been shown that a thin layer of NiO in a spintronic device can be used to transport spin current between two layers while blocking charge current [25–30] and that NiO can be used to generate radiation with THz frequency in spin-torque nano-oscillators [44]. Considering the long tradition of attention to NiO, one would expect that all of its basic properties have been studied in some detail. However, this does not apply to one of the characteristic features of antiferromagnets, the spin-flop transition.

As is well known, when a magnetic field is applied along the direction of the spins in a two-sublattice AF, as the field increases and exceeds a critical value H_{SF}, the spins of both sublattices suddenly rotate and align almost perpendicular to the field in a canted, spin-flop (SF) state [45–47]. This is a first-order transition that has been studied in detail in AF materials with easy axis anisotropy, such as the insulating fluorides MnF_2 and FeF_2 that crystallize in the tetragonal rutile structure, with the sublattice spins along the [001] axis. Their magnetic interactions are dominated by nearest-neighbor exchange, having effective exchange fields on the same order of magnitude, $H_E = 515$ and 540 kOe, respectively, for MnF_2 and FeF_2, and consequently similar Néel temperatures, $T_N \approx 67$ and 78 K [47]. However, their magnetic anisotropies differ by several orders of magnitude. In MnF_2 the anisotropy is due to dipolar interactions and is relatively weak, with effective anisotropy field $H_A \approx 10$ kOe [48], while in FeF_2 it arises from crystal-field and spin-orbit interactions and is represented by $H_A = 190$ kOe [49,50]. With a magnetic field H_0 applied along the easy axis, for $H_A \ll H_E$ and at low temperatures, the frequencies of the two $k \approx 0$ magnon modes, or antiferromagnetic resonance (AFMR), are given by $\omega_0 \approx \gamma \sqrt{2 H_E H_A} \pm \gamma H_0$, where γ is the gyromagnetic ratio. Thus, as the field increases, the frequency of the low-lying mode goes to zero and it becomes unstable when the field exceeds the critical value $H_{SF} \approx \sqrt{2 H_E H_A}$, characterizing the limit of stability of the AF phase and the onset of the spin-flop transition. In MnF_2 the AFMR frequency measured by far-infrared absorption at zero field is 261 GHz [51], and the measured SF field is $H_{SF} \approx 93$ kOe [21,52], consistent with the value $\gamma = 2.8$ GHz/kOe. In FeF_2 the AFMR frequency is 1.58 THz [49,53] and its spin-flop transition occurs at $H_{SF} \approx 500$ kOe, corresponding to $\gamma = 3.16$ GHz/kOe [54]. NiO is characterized by two distinct anisotropies, a negative one (hard) along $\langle 111 \rangle$ axes that forces the spins to lie in {111} planes and a positive in-plane one (easy) along $\langle 11\bar{2} \rangle$ axes. Thus, one would expect that when a field is applied in the easy plane along the easy axis, there would be a spin-flop transition at a field $H_{SF} = \sqrt{2 H_E H_{Az}}$, where H_{Az} is the in-plane anisotropy field.

The present investigation was motivated by the fact that for NiO there is considerable discrepancy in the estimated values for the spin-flop field and also in the scarce experimental data. Based on the parameters obtained from the data of

*Corresponding author: rezende@df.ufpe.br

Ref. [35], the spin-flop field at room temperature has been estimated to be 90 kOe in Ref. [37] and 85 kOe in Ref. [38]. Measurements by optical techniques [55] and magnetic torque [56] have led to room-temperature critical field values of 15.4 and 16.0 kOe, respectively. On the other hand, with the values $H_E = 9684$ kOe and $H_{Az} = 0.11$ kOe obtained from the fit of calculations to measured magnon frequencies [57] we find $H_{SF} = 46.2$ kOe, which is quite different from all previous numbers. The difficulties in determining the spin-flop field in NiO arise mainly from the fact that in bulk crystals there are AF domains with spins in 12 different directions [55,56,58] and the transition is quite sensitive to the angle between the applied field and the spins [52]. Thus, since it is unavoidable to have many domains in a sample, even if the field is applied along the easy axis of a specific domain, its response to the probing excitation competes with that of the other domains. Of course the difficulty persists with thin films, because they are textured, i.e., with a random orientation of AF easy axes.

In this paper we present an experimental and theoretical study of the spin-flop transition in a single-crystal sample of NiO. The temperature dependence of the critical field is obtained from measurements of the magnetic susceptibility. Since the limit of stability of the AF phase is characterized by the field at which the frequency of the low-lying $k = 0$ magnon frequency goes to zero, the phase boundary is calculated with spin-wave theory considering the renormalization of the magnon energies due to four-magnon processes arising from the exchange and anisotropy interactions. The calculated temperature dependence of the spin-flop field is in good agreement with the experimental data in the temperature range 5–325 K, where the spin-wave theory is expected to be accurate.

II. EXPERIMENTS

The experiments described in this section were performed with a NiO sample with the shape of a slab with dimensions $4 \times 2 \times 1$ mm^3, cut from a commercial single-crystal 1-mm-thick disk with the face in the (111) crystallographic plane. The magnetization M and the ac susceptibility χ_{ac} were measured using the ac/dc magnetometry system (ACMS) modulus of a Quantum Design physical property measurement system (PPMS). The ACMS sensitivities for measuring magnetic moments with the dc and ac setups are, respectively, 2.5×10^{-5} emu and 1.0×10^{-8} emu. These values are three to four orders of magnitude smaller than the level of the signal detected in our measurements. Both ac and dc magnetic fields were applied in the (111) plane parallel to the sample surface. The sample temperature T was varied in the range 5–325 K. In all measurements the temperature was stabilized to within ± 0.01 K. The applied magnetic field was swept from -85 to 85 kOe with various steps: 2 kOe for $85 > |H_0| > 20$ kOe; 1 kOe for $20 > |H_0| > 1$ kOe; and 0.1 kOe for $|H_0| < 1$ kOe. In the ac susceptibility mode, at each magnetic field step, the system was set to average the χ_{ac} data performing 133 measurements. This mode is important for determining the standard deviation (SD) of the measurements, which is an indication of the size of the fluctuations in the χ_{ac} data. The SD data, among others, are readily given by the PPMS measurement data file together with the in-phase and out-of-phase components of χ_{ac}.
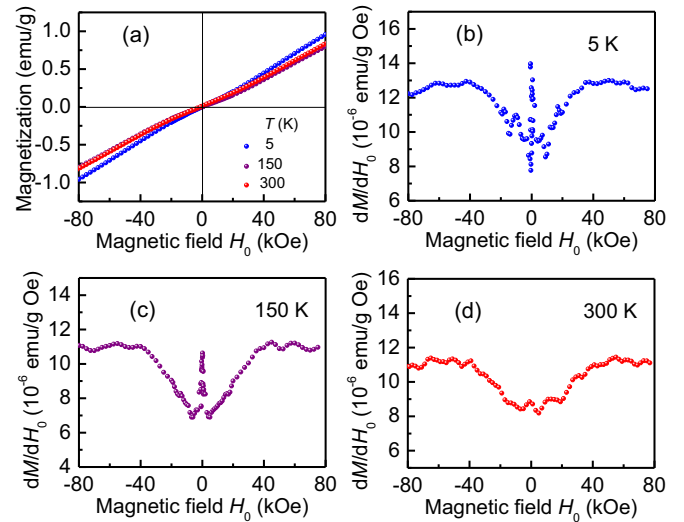

FIG. 1. (a) Measured variation of the magnetization of NiO with applied magnetic field at three temperatures T indicated; (b)–(d) are the corresponding dc susceptibilities obtained numerically with dM/dH_0.

The magnetization and susceptibility measurements were done at various field directions in the (111) plane revealing the expected threefold symmetry. The sharpest transitions, presented later, were observed with the field parallel to the [11$\bar{2}$] axis, determined by x-ray diffraction, which is one of the three easy axes in the plane. Thus, the results presented here refer only to this field direction. Figure 1(a) shows the variation of the magnetization M with magnetic field H_0 measured at three temperatures 5, 150, and 300 K, which are well below the Néel temperature $T_N = 523$ K. At all temperatures one observes a change in slope of the $M(H_0)$ curves around 40 kOe. This is seen more clearly in the dc susceptibility dM/dH_0 data obtained numerically and shown in Figs. 1(b)–1(d). As will be shown later, the increase in the magnetization at $H_0 < 40$ kOe is due to the rotation of the spins in the domains along the other two $\langle 11\bar{2} \rangle$ directions in the plane, at 120° with the field. The spin-flop transition that occurs in the range $40 < H_0 < 80$ kOe produces little change in the magnetization. This is due to the fact that in the SF transition the oppositely aligned spins in the AF phase flip to nearly oppositely aligned perpendicular to the field in the SF phase. Thus, the magnetization data do not allow the measurement of the SF field in NiO, as done for other AF materials [45,59–62]. The noisy central peak in Figs. 1(b) and 1(c) is attributed to the motion of the so-called S-domain walls that occurs at low fields [55,56,63].

A very convenient and accurate method to determine the AF-SF boundary consists of sweeping the applied field and measuring the ac susceptibility at constant temperature. This has been done with an ac field parallel to the static field, with frequency f and magnitude h_{ac} of, respectively, 1 kHz and 10.0 Oe. Figures 2(a), 2(c), and 2(e) show the field dependence of the real part of the ac susceptibility $\chi'(H_0)$ of NiO measured at three temperatures, 5, 150, and 300 K. Again, the $\chi'(H_0)$ data do not exhibit a clear indication of the AF-SF at any temperature. However, the data for the standard deviation, shown in Figs. 2(b), 2(d), and 2(f) exhibit an abrupt change
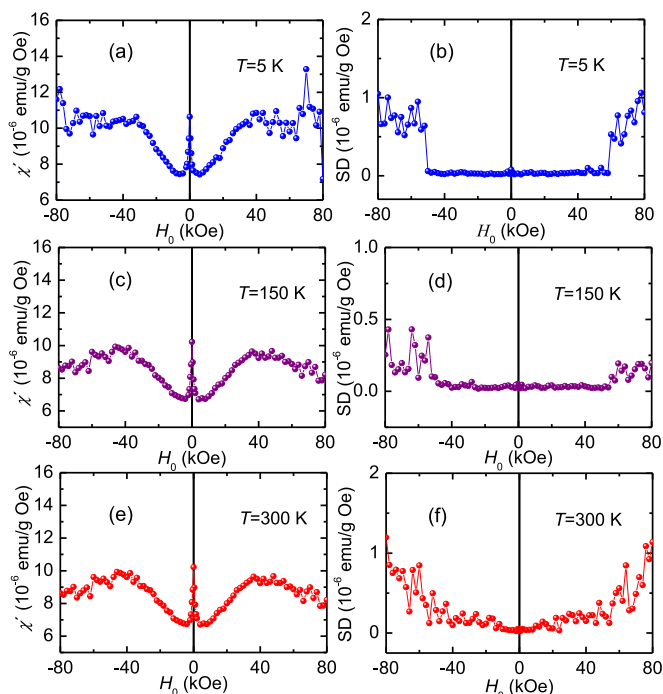
FIG. 2. (a),(c),(e) Variation with magnetic field of the real part of the ac susceptibility measured at the temperatures indicated; (b),(d),(f) standard deviation of the susceptibility measurement.

at a field that depends on the temperature and is indicative of the onset of the AF-SF transition. This is so because the AF-SF transition is of first order, in which the thermodynamic phase boundary lies between the limits of stability of the AF and of the SF phases [45,46]. As the applied field increases and exceeds the critical value for stability of the AF phase, the system enters in a regime of large fluctuations due to the formation of AF-SF domains walls that produce a series of discontinuous jumps in the magnetization and irreversible behavior [64,65]. Since the sum of the static and modulation fields drives the spin system back and forth across the energy barriers, the irreversibilities produce fluctuations in the ac susceptibility which reflects in the standard deviation data.

Figure 3 shows the measured AF-SF boundary obtained from the data in Fig. 2 by taking, at each temperature, the average of the absolute values of the two critical fields measured with decreasing and increasing field. The error bars were determined by the difference between the two values. At $T = 5$ K the critical field is $H_{SF} = 54 \pm 4$ kOe, which is larger than the values reported in [55,56] but much lower than the values estimated in [37,38]. As the temperature increases the critical field decreases, which is the opposite behavior to that observed in MnF_2 [21,52].

III. SEMICLASSICAL THEORY

In this section we present a semiclassical treatment of the macrospin response to an applied magnetic field in the plane of an easy-plane antiferromagnet. We consider various aspects of the questions involved in two subsections. The first is devoted to calculate the configuration of the sublattice macrospins based on energy arguments and in the second we calculate
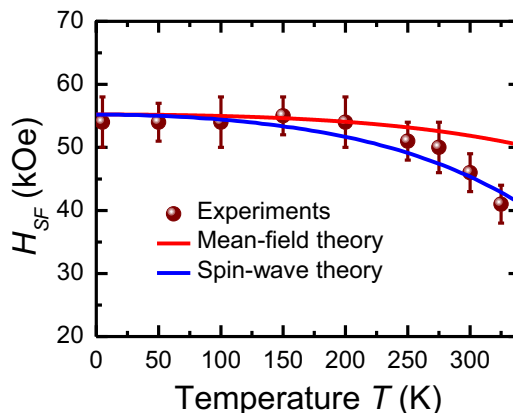

FIG. 3. Temperature dependence of the critical field for the AF-SF transition. Symbols represent the values measured from the change in behavior of the standard deviation of the ac susceptibility. The red solid curve represents the critical field calculated with mean-field theory presented in Sec. III and the blue line is the theoretical fit with the quantum spin-wave theory with four-magnon energy renormalization presented in Secs. IV and V.

the frequencies of the uniform spin precession corresponding to the antiferromagnetic resonance (AFMR) modes.

Above the Néel temperature $T_N = 523$ K, NiO has the sodium chloride structure with the Ni^{2+} and O^{2-} ions arranged in two face-centered-cubic lattices, as illustrated in Fig. 4(a). Below T_N, the spins of the Ni^{2+} ions are ordered ferromagnetically in {111} planes where they lie along $\langle 11\bar{2} \rangle$ directions, while the spins in adjacent {111} planes are oppositely aligned forming an AF arrangement [34,35]. Here we will ignore
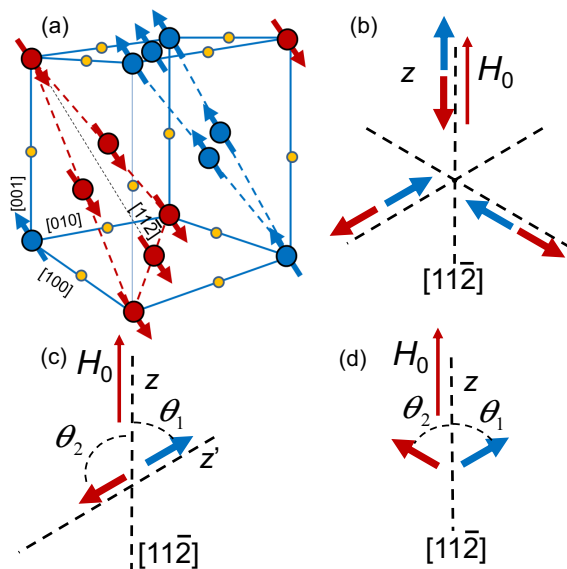

FIG. 4. (a) Crystal structure and spin arrangements in the antiferromagnetic phase of NiO. The small yellow circles represent O^{2-} ions and the large circles represent the Ni^{2+} ions. (b) Schematic representations of the AF spin domains in the {111} plane with the magnetic field H_0 applied along the direction of one of the domains. (c) Spin arrangement in a spin domain at an angle of $2\pi/3$ with the applied magnetic field H_0. (d) Spin arrangement in the spin-flop phase of a spin domain along the applied magnetic field H_0.

the small orthorombic distortion that occurs below T_N and consider the spins arranged in two AF sublattices. The spin Hamiltonian with Zeeman energy, exchange interaction, and out-of-plane (x) and in-plane (z) anisotropy energies can be written as [35]

$$H = -\gamma \hbar \sum_{i,j} H_0 S_{i,j}^z + \sum_{i,j} 2J_{ij} \vec{S}_i \cdot \vec{S}_j$$
$$+ \sum_{i,j} D_x \left(S_{i,j}^x \right)^2 - D_z \left(S_{i,j}^{z'} \right)^2, \qquad (1)$$

where $\vec{S}_i$ and $\vec{S}_j$ are, respectively, the spins (in units of $\hbar$) at sites i and j of sublattices 1 and 2, H_0 is the applied static magnetic field, J_{ij} is the exchange constant of the interaction between spins $\vec{S}_i$ and $\vec{S}_j$, $\gamma = g\mu_B/\hbar$ is the gyromagnetic ratio, g is the spectroscopic splitting factor, μ_B is the Bohr magneton, $\hbar$ is the reduced Planck constant, and $D_x > 0$ and $D_z > 0$ are the anisotropy constants, such that x is a hard direction along a $\langle 111 \rangle$ axis and z' is an easy direction along one of the three $\langle 11\bar{2} \rangle$ axes in the (111) plane. The Hamiltonian in Eq. (1) will be the basis for the calculations in the following subsections.

A. Macrospin configurations

We use a macrospin approximation and associate to $\vec{S}_i$ and $\vec{S}_j$ uniform sublattice magnetizations $\vec{M}_{1,2} = \gamma \hbar N \vec{S}_{i,j}$, where N is the number of spins per unit volume. For $T = 0$ the static sublattice magnetizations have the same value, $M_1 = M_2 = M$. In order to calculate the static spin response to a magnetic field H_0 applied along the z' direction of one of the spin domains, as sketched in Fig. 4(b), we use the energy per unit volume obtained from Eq. (1),

$$E = -H_0(M_{1z} + M_{2z}) + \frac{H_E}{M} \vec{M}_1 \cdot \vec{M}_2 + \frac{H_{Ax}}{2M} \left(M_{1x}^2 + M_{2x}^2 \right)$$
$$- \frac{H_{Az}}{2M} \left(M_{1z'}^2 + M_{2z'}^2 \right), \qquad (2)$$

where H_E, H_{Ax}, and H_{Az} are effective exchange and anisotropy fields defined by

$$H_E = 2SzJ/\gamma \hbar, \quad H_{Ax} = 2S D_x/\gamma \hbar, \quad H_{Az} = 2S D_z/\gamma \hbar, \qquad (3)$$

where we have considered only intersublattice exchange interaction between the z nearest neighbors with parameter J. Initially we use the energy in Eq. (2) to calculate the configuration of the spins in a domain at an angle $2\pi/3$ with the field, as in Fig. 4(c), so that the energy in Eq. (2) becomes

$$\frac{E(\theta_1, \theta_2)}{M} = -H_0(\cos\theta_1 + \cos\theta_2) + H_E \cos(\theta_1 + \theta_2)$$
$$- \frac{H_{Az}}{2} \cos^2\left(\frac{\pi}{3} - \theta_1\right) - \frac{H_{Az}}{2} \cos^2\left(2\frac{\pi}{3} - \theta_2\right). \qquad (4)$$

In order to introduce a temperature dependence in the calculation, we consider that in the temperature range of interest the interaction parameters in Eq. (1) are constants. Since the exchange and anisotropy effective fields in Eq. (3) are proportional to the spin S, in the spirit of the mean-field approximation we consider that they vary with the
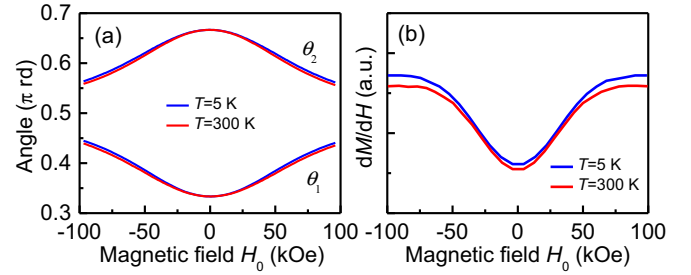

FIG. 5. (a) Calculated variation with magnetic field of the sublattice spin angles in the spin domains at an angle of $\pm 2\pi/3$ with the field, as in Fig. 4(c), for the two temperatures indicated. (b) Variation with field of slope of $M(H_0)$ due to a spin domain at an angle with the field, as in Fig. 4(c).

sublattice magnetization, $M(T) \propto \langle S \rangle$. A polynomial fit to the magnetization data of Roth [34] in the temperature range 0–400 K gives the factor $F_M(T) = M(T)/M(0) = 1 - 0.11 (T/T_N)^2 - 0.23 (T/T_N)^4$. This is used to express the temperature dependence of the fields as $H_{E,Az}(T) = F_M(T) H_{E,Az}$. Equation (4) was numerically evaluated by varying the angles θ_1, θ_2 in the range 0–π to find the values that minimize the energy for a given magnetic field, which is varied in steps of 0.5 kOe in the range -100 to $+100$ kOe. Figure 5 shows the results obtained for NiO using for the effective fields $H_E = 9684$ kOe, $H_{Az} = 0.3$ kOe, that will be justified later. As shown in Fig. 5(a), as the field increases the sublattice spins rotate gradually so as to maintain an angle between them of $\theta_1 + \theta_2 \approx \pi$, imposed by the very large exchange field. As a result, the total magnetization in the field direction $M_z = M(T)\cos\theta_1 + M(T)\cos\theta_2$ increases with field with a slope that changes in the field range -50 to $+50$ kOe as shown in Fig. 5(b). This result is in good agreement with the experimental data of Fig. 2 and confirms that the change in the slope of the magnetization, observed experimentally, is produced by the rotation of the spin domains that are at an angle of $\pm 2\pi/3$ with the field. Note that the calculated field dependencies of the angles and the magnetization for $T = 0$ and 300 K are very similar, in agreement with the experimental data of Fig. 1.

Next we consider the response of the spins in the domain lying along the field direction. The equation for minimum energy has two solutions, one for the antiferromagnetic (AF) phase and one for the spin-flop (SF) phase. In the AF phase, illustrated in Fig. 4(b), the angles are $\theta_1 = 0$, $\theta_2 = \pi$. Using these values in Eq. (2) we obtain the energy $E_{AF}/M = -H_E - H_{Az}$. In the SF phase, the spins are canted at angles $\theta_1 = \theta_2 = \theta$, illustrated in Fig. 4(d), and the energy obtained from Eq. (2) is

$$\frac{E_{SF}}{M} = -2H_0\cos\theta + H_E\cos 2\theta - H_{Az}\cos^2\theta. \qquad (5)$$

The angle of equilibrium, determined by $\partial E(\theta)/\partial\theta = 0$, is given by $\cos\theta = H_0/(2H_E - H_{Az})$. The configuration that prevails is the one with lower energy, so it depends on the relative values of the fields. Since for a certain material H_E and H_{Az} are fixed, the equilibrium configuration depends on the value of H_0. For fields below a critical value, the spins are in the AF phase. As the field increases and goes above the

value

$$H_{SF} = \left(2 H_E H_{Az} - H_{Az}^2\right)^{1/2}, \tag{6}$$

the energy $E_{SF} < E_{AF}$ and the spins flip to the canted position. Using for NiO the values $H_E = 9684\,\text{kOe}$, $H_{Az} = 0.3\,\text{kOe}$, we obtain with Eq. (6) $H_{SF} \approx \sqrt{2 H_E H_{Az}} = 76.2\,\text{kOe}$, a value quite larger than the experimental data. The reason for this discrepancy is the fact that at a field lower than the one given by Eq. (6), the frequency of one of the spin-wave modes goes to zero and the AF phase becomes unstable, as will be shown later. The temperature variation of the critical field in the mean-field model can be obtained considering in Eq. (6) the exchange and anisotropy fields multiplied by the magnetization factor $F_M(T)$ used earlier. In order to compare the temperature dependence with the experimental data, we use for $H_{SF}(0)$ the value 55.2 kOe, instead of 76.2 kOe. The result, represented by the red solid curve in Fig. 3, demonstrates that the experimental data cannot be explained by classical mean-field theory.

B. Antiferromagnetic resonance of the easy-plane AF

For the sake of completeness, and also to show the importance of quantum effects in the easy-plane antiferromagnet,

we now derive the frequencies of the uniform precession modes of the sublattice magnetizations. The equations of motion for the magnetization components are obtained from the Landau-Lifshitz equation

$$\frac{d\vec{M}_{1,2}}{dt} = \gamma \, \vec{M}_{1,2} \times \vec{H}_{\text{eff}\,1,2}, \tag{7}$$

where $\vec{H}_{\text{eff}\,1,2}$ represent the effective fields that act on the sublattice magnetizations, given by

$$\vec{H}_{\text{eff}\,1,2} = -\nabla_{\vec{M}_{1,2}} [E(\vec{M}_{1,2})]. \tag{8}$$

Writing for the magnetizations $\vec{M}_{1,2} = \hat{z}\,M_{1,2z} + (\hat{x}\,m_{1,2x} + \hat{y}\,m_{1,2y})\,e^{i\omega t}$ we obtain with Eqs. (7) and (8) the linearized equations of motion for the transverse components of the sublattice magnetizations. They can be written as an eigenvalue equation in matrix form,

$$[A](m) = i[\omega](m), \tag{9}$$

where $(m) = (m_{1x}, m_{2x}, m_{1y}, m_{2y})^T$ is a column matrix, $[\omega]$ is a diagonal matrix of the eigenvalues, and

$$[A] = \begin{bmatrix} 0 & 0 & [\gamma H_0 + (A - C)] & B \\ 0 & 0 & -B & [\gamma H_0 - (A - C)] \\ -[\gamma H_0 + (A + C)] & -B & 0 & 0 \\ B & -[\gamma H_0 - (A + C)] & 0 & 0 \end{bmatrix}, \tag{10}$$

where the parameters are defined by

$$A = \gamma \, [H_E + H_{Ax}/2 + H_{Az}], \tag{11a}$$

$$B = \gamma \, H_E, \tag{11b}$$

$$C = \gamma \, H_{Ax}/2. \tag{11c}$$

The AFMR frequencies are the eigenvalues of Eq. (9), that are given by the roots of $\det[A - i\omega] = 0$. Note that if there is no hard-axis anisotropy, $C = 0$, so Eqs. (9) and (10) are the same as the ones for an easy-axis antiferromagnet [66]. For the easy-plane AF the frequencies of the two AFMR modes are

$$\omega_{\alpha,\beta}^2 = \left(A^2 + \gamma^2 H_0^2\right) - (C^2 + B^2)$$
$$\pm 2\sqrt{\gamma^2 H_0^2 (A^2 - B^2) + B^2 C^2}. \tag{12}$$

Considering $H_E \gg H_{Ax} \gg H_{Az}$, appropriate for NiO, Eqs. (11) and (12) give

$$\omega_{\alpha,\beta}^2 \approx \gamma \left[\left(2 H_E H_{Az} + H_E H_{Ax} + H_0^2\right) \pm H_E H_{Ax} \pm 2 H_0^2\right], \tag{13}$$

so that the two frequencies are

$$\omega_{\alpha 0}^2 \approx \gamma \left(2 H_E H_{Ax} + 3 H_0^2\right), \tag{14}$$

$$\omega_{\beta 0}^2 \approx \gamma \left(2 H_E H_{Az} - H_0^2\right). \tag{15}$$

These expressions agree with two of the four frequencies obtained by [38] for zero-wave-vector spin waves in an

easy-plane AF using a Green's-function approach. The other two frequencies in [38] probably refer to another wave vector since in a two-sublattice AF there are only two spin-wave modes. Equation (15) shows that as the field increases, the β-mode frequency decreases and it goes to zero at the onset of the spin-flop phase at a field $H_{SF} \approx (2 H_E H_{Az})^{1/2}$, in agreement with the value obtained with energy considerations.

IV. QUANTUM THEORY OF INTERACTING SPIN WAVES

In this section we present a quantum formulation of interacting spin waves, which is essential to explain the temperature dependence of the spin-flop transition and other aspects of the experimental data. We consider the spin Hamiltonian in Eq. (1) and treat the quantized excitations of the magnetic system with the approach of Holstein-Primakoff [67,68], which consists of transformations that express the spin operators in terms of boson operators that create or annihilate the quanta of spin waves, magnons. In the first transformation the components of the local spin operators are related to the creation and annihilation operators of spin deviations for the two sublattice sites as

$$S_{1i}^+ = (2S)^{1/2} \left(1 - \frac{a_i^+ a_i}{2S}\right)^{1/2} a_i,$$

$$S_{1i}^- = (2S)^{1/2} a_i^+ \left(1 - \frac{a_i^+ a_i}{2S}\right)^{1/2}, \tag{16a}$$

$$S_{1i}^z = S - a_i^+ a_i,$$

$$S_{2j}^+ = (2S)^{1/2} b_j^+ \left(1 - \frac{b_j^+ b_j}{2S}\right)^{1/2},$$

$$S_{2j}^- = (2S)^{1/2} \left(1 - \frac{b_j^+ b_j}{2S}\right)^{1/2} b_j, \qquad (16b)$$

$$S_{2j}^z = -S + b_j^+ b_j,$$

where $a_i^\dagger$, a_i, and $b_j^\dagger$, b_j, are the creation, destruction operators for spin deviations at sites i, j of sublattices 1 and 2, which satisfy the boson commutation rules $[a_i, a_{i'}^\dagger] = \delta_{ii'}$, $[a_i, a_{i'}] = 0$, $[b_j, b_{j'}^\dagger] = \delta_{jj'}$ and $[b_j, b_{j'}] = 0$. The next step consists of introducing a transformation from the localized field operators to collective boson operators that satisfy the commutation rules $[a_k, a_{k'}^\dagger] = \delta_{kk'}$, $[a_k, a_{k'}] = 0$, $[b_k, b_{k'}^\dagger] = \delta_{kk'}$, $[b_k, b_{k'}] = 0$,

$$a_i = N^{-1/2} \sum_k e^{i\vec{k}\cdot\vec{r}_i} a_k, \quad b_j = N^{-1/2} \sum_k e^{i\vec{k}\cdot\vec{r}_j} b_k, \quad (17)$$

where N is the number of spins in each sublattice and $\vec{k}$ is a wave vector, with the orthonormality condition

$$N^{-1} \sum_i e^{i(\vec{k}-\vec{k}')\cdot\vec{r}_i} = \delta_{k,k'}. \qquad (18)$$

Introducing in Eq. (1) the transformations in Eqs. (16) with the binomial expansions of the square roots, and using Eqs. (17) and (18), we obtain a Hamiltonian with the form $H = E_0 + H^{(2)} + H^{(4)} + H^{(6)} \ldots$, where each term contains an even number of boson operators. The quadratic part of the Hamiltonian is

$$H^{(2)} = \gamma \hbar \left[H_0 \sum_k (a_k^+ a_k - b_k^+ b_k) \right.$$

$$+ \sum_k \gamma_k H_E (a_k b_{-k} + a_k^+ b_{-k}^+) + H_E (b_k^+ b_k + a_k^+ a_k)$$

$$+ \frac{H_{Ax}}{4} (a_k a_{-k} + a_k^+ a_{-k}^+ + a_k a_k^+ + a_k^+ a_k + b_k b_{-k}$$

$$\left. + b_k^+ b_{-k}^+ + b_k b_k^+ + b_k^+ b_k) + H_{Az} (a_k^+ a_k + b_k^+ b_k) \right],$$

$$(19)$$

where γ_k is a structure factor defined by $\gamma_k = (1/z) \sum_\delta \exp(i\vec{k}\cdot\vec{\delta})$, and $\vec{\delta}$ are the vectors connecting nearest neighbors. The quadratic Hamiltonian written in normal order and without the constants becomes

$$H = \hbar \sum_k (A + \gamma H_0) a_k^+ a_k + (A - \gamma H_0) b_k^+ b_k$$

$$+ B_k (a_k b_{-k} + a_k^+ b_{-k}^+) + \frac{1}{2} C (a_k a_{-k} + b_k b_{-k} + \text{H.c.}),$$

$$(20)$$

where the parameters A and C are the same defined in Eqs. (11) and $B_k = \gamma_k B$. Note that in Ref. [57] the in-plane anisotropy was taken in the y direction, which is inconsistent with the direction of equilibrium. For this reason the parameters A and C here are different from those in Ref. [57]. However, since the anisotropy energies are much smaller than exchange, at the end

the dispersion relations given in [57] are very approximately the same as the ones obtained here.

The next step consists of performing canonical transformations from the collective boson operators $a_k^\dagger, a_k, b_k^\dagger, b_k$ into magnon creation and annihilation operators $\alpha_k^\dagger, \alpha_k, \beta_k^\dagger, \beta_k$ such that the quadratic Hamiltonian is cast in the diagonal form

$$H^{(2)} = \sum_k \hbar (\omega_{\alpha k} \alpha_k^+ \alpha_k + \omega_{\beta k} \beta_k^+ \beta_k), \qquad (21)$$

where $\omega_{\alpha k}$ and $\omega_{\beta k}$ are the frequencies of the two magnon modes. Following [57] one can show that the unrenormalized magnon frequencies are

$$\omega_{\alpha,\beta}^2 = (A^2 + \gamma^2 H_0^2) - (C^2 + B_k^2)$$

$$\pm 2\sqrt{\gamma^2 H_0^2 (A^2 - B_k^2) + B_k^2 C^2}. \qquad (22)$$

This equation has the same form as Eq. (12) obtained with the semiclassical approach for the uniform mode. Here the presence of B_k instead of B makes it valid for any wave vector.

Equation (22) represents the magnon energies without magnon interactions that are described by terms with more than two operators. The magnon interactions have two important effects, to renormalize the energies and to introduce damping [68,69]. The interactions of lowest order arise from terms in the Hamiltonian containing four boson operators, $a_k^\dagger, a_k, b_k^\dagger, b_k$, originating from both the exchange and anisotropy energies. In order to write these terms with the magnon operators $\alpha_k^\dagger, \alpha_k, \beta_k^\dagger, \beta_k$ we use approximate canonical transformation [57,70] valid for $C \ll A, B_k$, as is the case of NiO that has $H_{Ax} \ll H_E$,

$$a_k = u_{\alpha k} \alpha_k - v_{\beta k} \beta_{-k}^\dagger, \qquad (23a)$$

$$b_{-k}^\dagger = -v_{\alpha k} \alpha_k + u_{\beta k} \beta_{-k}^\dagger, \qquad (23b)$$

where the parameters $u_{\alpha,\beta k}$ and $v_{\alpha,\beta k}$ are

$$u_{\alpha,\beta k} = \left(\frac{A + \omega_{\alpha,\beta k}}{2\omega_{\alpha,\beta k}(0)}\right)^{1/2}, \quad v_{\alpha,\beta k} = \left(\frac{A - \omega_{\alpha,\beta k}}{2\omega_{\alpha,\beta k}(0)}\right)^{1/2}, \quad (24)$$

where $\omega_{\alpha,\beta k}(0)$ are the frequencies of the two modes with $H_0 = 0$. Among the many terms in the Hamiltonian with four magnon operators, we retain only those that have pairs of creation-annihilation operators for the same mode, in any order, such as $\alpha_{k1}^\dagger \alpha_{k2}^\dagger \alpha_{k3}^\dagger \alpha_{k4}$, $\alpha_{k1}^\dagger \alpha_{k2}^\dagger \beta_{k3}^\dagger \beta_{k4}$, and $\beta_{k1} \beta_{k2}^\dagger \beta_{k3}^\dagger \beta_{k4}$. Then we use a random-phase approximation to replace one of the pairs by its thermal average such that the term has the form as in Eq. (21). For example, $\alpha_{k1}^\dagger \alpha_{k2}^\dagger \beta_{k3}^\dagger \beta_{k4} \Delta(\vec{k}_1 + \vec{k}_4 - \vec{k}_2 - \vec{k}_3)$ is replaced by $\langle \alpha_q \alpha_q^\dagger \rangle \beta_k^\dagger \beta_k = (\bar{n}_{\alpha q} + 1) \beta_k^\dagger \beta_k + \bar{n}_{\beta q} \alpha_k^\dagger \alpha_k$, where $\bar{n}_{\alpha,\beta q}$ is the thermal occupation number of the α or β mode with wave vector $\vec{q}$, given by the Bose-Einstein distribution $\bar{n}_{\alpha,\beta q} = 1/(e^{\hbar\omega_{\alpha,\beta q}/k_B T} - 1)$. The averages of other pairs of operators such as $\alpha_{k1} \alpha_{k2} \beta_{k3}^\dagger \beta_{k4}$ or $\alpha_{k1} \alpha_{k3}^\dagger \beta_{k2} \beta_{k4}$ vanish or do not contribute to the energy of either mode. Applying this approximation to each four-magnon term, the Hamiltonian reduces to a quadratic form

$$H_{ex}^{(4)} \Rightarrow \hbar \sum_k \Delta\omega_{\alpha k} \alpha_k^\dagger \alpha_k + \Delta\omega_{\beta k} \beta_k^\dagger \beta_k, \qquad (25)$$

where $\hbar \Delta \omega_{\alpha k}$ and $\hbar \Delta \omega_{\beta k}$ represent the renormalization of the energies of the two modes, so that the total magnon energies become temperature dependent, $\hbar \omega_{\alpha,\beta k}(T) + \hbar \Delta \omega_{\alpha,\beta k}(T)$. Using the contributions from the exchange and hard-axis anisotropy interactions, the total four-magnon contribution to the β-mode energy becomes

$$
\begin{aligned}
\hbar \Delta \omega_{\beta k}(T) = zJ \big[&\big(u_{\beta k}^2 + v_{\beta k}^2 - 2u_{\beta k}v_{\beta k}\gamma_k\big)C_q \\
&+ \big(u_{\beta k}v_{\beta k}\gamma_k - v_{\beta k}^2\big)E_q + \big(u_{\beta k}v_{\beta k}\gamma_k - u_{\beta k}^2\big)F_q \big] \\
&- D_x \big(u_{\beta k}^2 G_q + v_{\beta k}^2 H_q\big),
\end{aligned}
\tag{26}
$$

where

$$
C_q = \frac{1}{N}\sum_q u_{\alpha q}v_{\alpha q}\gamma_q\,(2\bar{n}_{\alpha q}+1) + u_{\beta q}v_{\beta q}\gamma_q\,(2\bar{n}_{\beta q}+1),
\tag{27a}
$$

$$
E_q = \frac{2}{N}\sum_q u_{\beta q}^2\,\bar{n}_{\beta q} + v_{\alpha q}^2\,(\bar{n}_{\alpha q}+1),
\tag{27b}
$$

$$
F_q = \frac{2}{N}\sum_q u_{\alpha q}^2\,\bar{n}_{\alpha q} + v_{\beta q}^2\,(\bar{n}_{\beta q}+1),
\tag{27c}
$$

$$
G_q = \frac{1}{2N}\sum_q u_{\beta q}^2(4\bar{n}_{\beta q}+1) + v_{\alpha q}^2(4\bar{n}_{\alpha q}+3),
\tag{27d}
$$

$$
H_q = \frac{1}{2N}\sum_q u_{\alpha q}^2(4\bar{n}_{\alpha q}+1) + v_{\beta q}^2(4\bar{n}_{\beta q}+3).
\tag{27e}
$$

The correction for the frequency of the α mode is given by the same expressions as (26) and (27) with the interchange $\alpha \leftrightarrow \beta$. In Eq. (26) we have neglected the contribution from the easy-axis anisotropy, as given in Ref. [71], because it is very small in NiO. It is important to note that even at $T = 0$ there is a correction to the magnon energies due to the magnon interactions. This zero-point correction is a characteristic feature of antiferromagnets that was noted by Oguchi several decades ago [72]. The Oguchi correction refers only to the contribution from the four-magnon interaction arising from exchange. While it is unimportant in many three-dimensional AFs, it has been shown to be essential to explain the observed magnon frequencies in one-dimensional AFs with Haldane gap [73]. As will be shown later, the (exchange) Oguchi correction is also negligible in NiO. However, the hard-axis anisotropy counterpart of the Oguchi zero-point correction to the β-mode energy is quite large in NiO. Using $\bar{n}_{\beta q} = \bar{n}_{\alpha q} = 0$ in Eqs. (26) and (27) and replacing the anisotropy parameter by the effective field using Eq. (3), we obtain for the anisotropy zero-point correction

$$
\begin{aligned}
\Delta \omega_{\beta k}(0) \approx \frac{-\gamma H_{Ax}}{4SN}\bigg[&u_{\beta k}^2 \sum_q \big(u_{\beta q}^2 + 3v_{\alpha q}^2\big) \\
&+ v_{\beta k}^2 \sum_q \big(u_{\alpha q}^2 + 3v_{\beta q}^2\big) \bigg].
\end{aligned}
\tag{28}
$$

In easy-plane antiferromagnets with $H_E \gg H_{Ax} \gg H_{Az}$, $u_{\beta 0} \approx v_{\beta 0} \gg 1$ so that the zero-point correction for the $k = 0$ β-mode energy can be quite large.

V. TEMPERATURE DEPENDENCE OF THE SF-PHASE BOUNDARY IN NiO

The renormalized energies of the two magnon modes were calculated numerically for NiO, for arbitrary wave vector k, temperature T, and field H_0. This was done by assuming a spherical Brillouin zone and converting the sums in Eqs. (27) into integrals in k space in the usual manner,

$$
\frac{1}{N}\sum_k \Rightarrow \frac{a^3}{(2\pi)^3}\int d^3k = \frac{a^3}{2\pi^2}\int_0^{k_{\max}} k^2 dk,
\tag{29}
$$

where a is the lattice parameter and k_m is the radius of the spherical Brillouin zone, an adjustable parameter chosen to fit the experimental data. We use for the structure factor $\gamma_k = \cos(\pi k / 2k_m)$, and the following parameters for NiO: $2SzJ/\gamma\hbar = H_E = 9684$ kOe, $2S D_x/\gamma\hbar = H_{Ax} = 6.35$ kOe, $H_{Az} = 0.3$ kOe, $g = 2.18$, and $k_{\max} = 0.445\,\pi/a$. The exchange and hard-axis anisotropy fields are the same used in Ref. [57], which are the values that fit the experimental data for the spin-wave dispersion [35] and the $k = 0$ frequency for the α mode [43]. The value of H_{Az} is larger than the one used in [57] because here we include the effect of the zero-point correction.

The temperature dependence of the spin-wave spectrum in NiO due to four-magnon interactions was calculated numerically by solving Eqs. (22) and (26)–(28) self-consistently for each value of temperature and field. The procedure consists of initially calculating the parameters in Eqs. (27) with the unrenormalized frequencies given by Eq. (22). Then at each point k in the Brillouin zone the renormalized magnon frequencies for both modes are calculated. The thermal occupation numbers are then computed with the renormalized frequencies, new coefficients and new frequencies are calculated, and the process is repeated until all changes in frequency throughout the Brillouin zone are smaller than a desired value, typically 0.3 GHz. Note that the temperature dependence of the magnon energies is entirely due to the thermal occupation numbers, since the energy renormalization in Eq. (26) depends on the exchange and anisotropy parameters, not on the effective fields, which are considered constants in the temperature range of interest.

The renormalized magnon frequencies in NiO, calculated for two temperatures, 5 and 300 K, in zero field, are shown in Fig. 6(a) over the whole Brillouin zone as a function of the reduced wave number $q = k/k_m$. The dispersion curves over most of the Brillouin zone at both temperatures are nearly the same. Figure 6(b) showing a zoom near the zone center reveals that while the renormalization is very small for the α mode, it is relatively large for the β mode for $k < 0.1\,k_m$. This can be understood by the examination of Eqs. (26) and (27) and the behavior of the parameters u and v of the canonical transformations (23). The dependencies of u and v on the wave vector for the two modes calculated with Eq. (24) are plotted in Figs. 6(c) and 6(d). With $H_E \gg H_{Ax} \gg H_{Az}$, for $k = 0$ we have from (24) $u_{\alpha 0} \approx v_{\alpha 0} \approx (H_E/8H_{Ax})^{1/4} \approx 3.72$ and $u_{\beta 0} \approx v_{\beta 0} \approx (H_E/8H_{Az})^{1/4} \approx 7.97$. Since $\gamma_0 = 1$, the terms multiplying H_E in Eq. (26) nearly cancel out so that the contribution of the four-magnon exchange interaction to the energy renormalization is negligible. Thus, although the anisotropy interaction is three orders of magnitude smaller than exchange, its contribution to the renormalization is enhanced
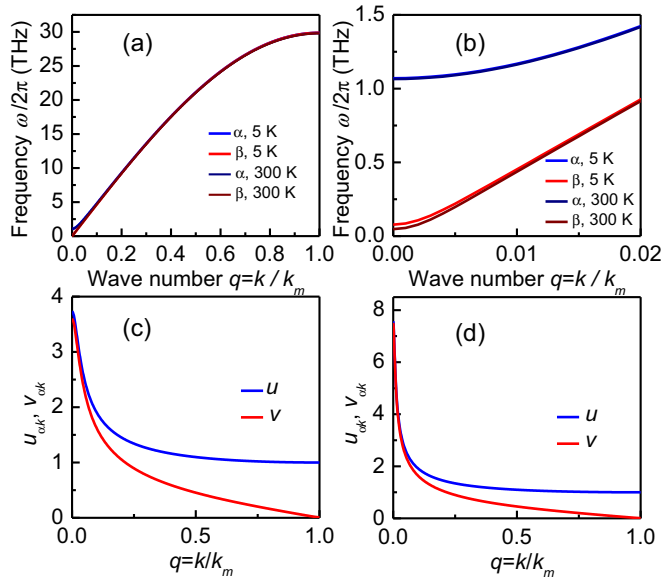
FIG. 6. (a) Magnon dispersion relations in antiferromanetic NiO calculated with four-magnon renormalization at $T = 5$ and 300 K. (b) Blow up of the Brillouin zone center showing the separation of the frequencies of the α (upper blue curve) and β (lower red curve) magnon modes. (c), (d) Variation with wave vector of the parameters u and v of the canonical transformations to magnon operators for the two modes.

at $k \approx 0$, and becomes significant. The energy renormalization is negative for both modes, and is larger for the β mode. Since $\omega_{\beta 0} \approx 0.1 \, \omega_{\alpha 0}$, the relative change of the β-mode frequency due to the renormalization is larger than for the α mode. As the wave vector increases, the parameters u and v as well as γ_k decrease fast, so that the renormalization at $T = 300$ K becomes unimportant. Notice that the zero-point correction for the $k = 0$ β-mode frequency, given by Eq. (28), is $\Delta\omega_{\beta 0}(0) \approx -0.15$ THz. This is a very large relative correction, 65% of the frequency without magnon interactions, $\omega_{\beta 0} = \gamma \sqrt{2H_E H_{Az}} = 0.23$ THz. The frequency with the zero-point correction is $\omega_{\beta 0}(0) = 0.08$ THz, which is an average of the two values measured with Brillouin light scattering [40].

Since the β-mode frequency decreases with increasing magnetic field, the field value for which the frequency goes to zero determines the limit of stability of the AF phase and hence the onset of the AF-SF transition. Figure 7 shows the variation with field intensity of the $k = 0$ frequency for the β-mode magnon calculated for three temperature values with four-magnon renormalization as described. The decrease in frequency with increasing temperature is due to four-magnon anisotropy interactions and has negligible influence of the exchange interaction.

The AF-SF phase boundary for NiO was obtained by determining the value of $H_0(T)$ for which the renormalized $\omega_{\beta 0}(T)$ becomes zero. The blue solid line in Fig. 3 shows the
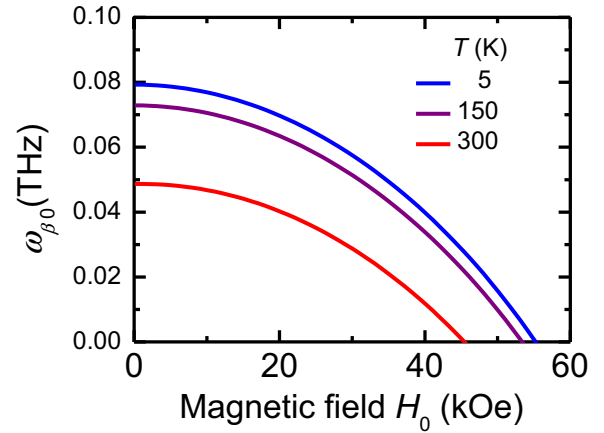

FIG. 7. Variation of the $k = 0$ down-going magnon frequency with applied field for various temperature values in NiO. The field value for which the frequency goes to zero determines the limit of the AF phase and onset of the AF-SF transition.

result of the calculation of the renormalized energies based on exchange and anisotropy four-magnon interactions. The agreement between theory and experiments is quite good in the temperature range of Fig. 3. At higher temperatures the theory can certainly be improved by considering the contributions from six-magnon interactions to the energy renormalization [68]. As previously remarked, the AF-SF transition is of first order and the thermodynamic phase boundary lies between the limits of stability of the AF and of the SF phases. As the applied field increases and exceeds the critical value for stability of the AF phase, given by the solid line in Fig. 3, the system enters in a regime of large fluctuations, so that the field range in which the AF-SF takes place can be detected by measuring the deviations in the ac susceptibility. As the field increases further, the system should reach the full SF phase where the fluctuations are expected to decrease. In NiO this occurs at fields above 85 kOe and could not be detected in our experiments.

[1] A. S. Núñez, R. A. Duine, P. Haney, and A. H. MacDonald, Phys. Rev. B **73**, 214426 (2006).

[2] A. B. Shick, S. Khmelevskyi, O. N. Mryasov, J. Wunderlich, and T. Jungwirth, Phys. Rev. B **81**, 212409 (2010).

[3] A. H. MacDonald and M. Tsoi, Phil. Trans. R. Soc. A **369**, 3098 (2011).

[4] V. M. T. S. Barthem, C. V. Colin, H. Mayaffre, M.-H. Julien, and D. Givord, Nat. Commun. **4**, 2892 (2013).

[5] E. V. Gomonay and V. M. Loktev, Low Temp. Phys. **40**, 17 (2014).

[6] R. Macêdo and T. Dumelow, Phys. Rev. B **89**, 035135 (2014).

[7] J. Železný, H. Gao, K. Výborný, J. Zemen, J. Mašek, A. Manchon, J. Wunderlich, J. Sinova, and T. Jungwirth, Phys. Rev. Lett. **113**, 157201 (2014).

[8] R. Cheng, J. Xiao, Q. Niu, and A. Brataas, Phys. Rev. Lett. **113**, 057601 (2014).

[9] V. Tshitoyan, C. Ciccarelli, A. P. Mihai, M. Ali, A. C. Irvine, T. A. Moore, T. Jungwirth, and A. J. Ferguson, Phys. Rev. B **92**, 214406 (2015).

[10] T. Jungwirth, X. Marti, P. Wadley, and J. Wunderlich, Nat. Nanotechnol. **11**, 231 (2016).

[11] V. Baltz, A. Manchon, M. Tsoi, T. Moriyama, T. Ono, and Y. Tserkovnyak, arXiv:1606.04284 [Rev. Mod. Phys. (2017) (to be published)].

[12] E. E. Fullerton and J. R. Childress, Proc. IEEE **104**, 1787 (2016).

[13] J. Nogués and I. K. Schuller, J. Magn. Magn. Mater. **192**, 203 (1999).

[14] J. R. Fermin, M. A. Lucena, A. Azevedo, F. M. de Aguiar, and S. M. Rezende, J. Appl. Phys. **87**, 6421 (2000).

[15] H. Chen, Q. Niu, and A. H. MacDonald, Phys. Rev. Lett. **112**, 017205 (2014).

[16] J. B. S. Mendes, R. O. Cunha, O. Alves Santos, P. R. T. Ribeiro, F. L. A. Machado, R. L. Rodriguez-Suarez, A. Azevedo, and S. M. Rezende, Phys. Rev. B **89**, 140406(R) (2014).

[17] W. Zhang, M. B. Jungfleisch, W. Jiang, J. E. Pearson, A. Hoffmann, F. Freimuth, and Y. Mokrousov, Phys. Rev. Lett. **113**, 196602 (2014).

[18] Y. Ou, S. Shi, D. C. Ralph, and R. A. Buhrman, Phys. Rev. B **93**, 220405(R) (2016).

[19] Y. Ohnuma, H. Adachi, E. Saitoh, and S. Maekawa, Phys. Rev. B **87**, 014423 (2013).

[20] S. Seki, T. Ideue, M. Kubota, Y. Kozuka, R. Takagi, M. Nakamura, Y. Kaneko, M. Kawasaki, and Y. Tokura, Phys. Rev. Lett. **115**, 266601 (2015).

[21] S. M. Wu, W. Zhang, K. C. Amit, P. Borisov, J. E. Pearson, J. S. Jiang, D. Lederman, A. Hoffmann, and A. Bhattacharya, Phys. Rev. Lett. **116**, 097204 (2016).

[22] S. M. Rezende, R. L. Rodríguez- Suárez, and A. Azevedo, Phys. Rev. B **93**, 014425 (2016).

[23] R. Cheng, S. Okamoto, and D. Xiao, Phys. Rev. Lett. **117**, 217202 (2016).

[24] P. Merodio, A. Ghosh, C. Lemonias, E. Gautier, U. Ebels, M. Chshiev, H. Béa, V. Baltz, and W. E. Bailey, Appl. Phys. Lett. **104**, 032406 (2014).

[25] H. Wang, C. Du, P. C. Hammel, and F. Yang, Phys. Rev. Lett. **113**, 097202 (2014).

[26] C. Hahn, G. de Loubens, V. V. Naletov, J. Ben Youssef, O. Klein, and M. Viret, Europhys. Lett. **108**, 57005 (2014).

[27] H. Wang, C. Du, P. C. Hammel, and F. Yang, Phys. Rev. B **91**, 220410(R) (2015).

[28] T. Moriyama, S. Takei, M. Nagata, Y. Yoshimura, N. Matsuzaki, T. Terashima, Y. Tserkovnyak, and T. Ono, Appl. Phys. Lett. **106**, 162406 (2015).

[29] W. Lin, K. Chen, S. Zhang, and C. L. Chien, Phys. Rev. Lett. **116**, 186601 (2016).

[30] T. Shang *et al.*, Appl. Phys. Lett. **109**, 032410 (2016).

[31] X. Marti *et al.*, Nat. Mater. **13**, 367 (2014).

[32] P. Wadley *et al.*, Science **351**, 587 (2016).

[33] T. Satoh, R. Iida, T. Higuchi, M. Fiebig, and T. Shimura, Nat. Photon. **9**, 25 (2014).

[34] W. L. Roth, Phys. Rev. **110**, 1333 (1958).

[35] M. T. Hutchings and E. J. Samuelsen, Phys. Rev. B **6**, 3447 (1972).

[36] R. D. McMichael, M. D. Stiles, P. J. Chen, and W. F. Egelhoff Jr., J. Appl. Phys. **83**, 7037 (1998).

[37] J. Nogués *et al.*, Appl. Phys. Lett. **82**, 3044 (2003).

[38] M. G. Cottam and A. L. Awang, J. Phys. C: Solid State Phys. **12**, 105 (1979); A. L. Awang and M. G. Cottam, *ibid.* **12**, 121 (1979).

[39] M. Grimsditch, L. E. McNeil, and D. J. Lockwood, Phys. Rev. B **58**, 14462 (1998).

[40] J. Milano, L. B. Steren, and M. Grimsditch, Phys. Rev. Lett. **93**, 077601 (2004).

[41] N. P. Duong, T. Satoh, and M. Fiebig, Phys. Rev. Lett. **93**, 117402 (2004).

[42] T. Satoh, S.-J. Cho, R. Iida, T. Shimura, K. Kuroda, H. Ueda, Y. Ueda, B. A. Ivanov, F. Nori, and M. Fiebig, Phys. Rev. Lett. **105**, 077402 (2010).

[43] T. Kampfrath, A. Sell, G. Klatt, A. Pashkin, S. Mährlein, T. Dekorsy, M. Wolf, M. Fiebig, A. Leitenstorfer, and R. Huber, Nat. Photon. **5**, 31 (2010).

[44] R. Cheng, D. Xiao, and A. Brataas, Phys. Rev. Lett. **116**, 207603 (2016).

[45] S. Foner, in *Magnetism*, edited by G. T. Rado and H. Suhl (Academic Press, Inc., New York, 1963), Vol. I, Chap. 9, p. 384.

[46] F. B. Anderson and H. B. Callen, Phys. Rev. **136**, A1068 (1964).

[47] L. J. de Jongh and A. R. Miedema, Adv. Phys. **50**, 947 (2001).

[48] J. Barak, V. Jaccarino, and S. M. Rezende, J. Magn. Magn. Mater. **9**, 323 (1978).

[49] R. C. Ohlmann and M. Tinkham, Phys. Rev. **123**, 425 (1961).

[50] M. T. Hutchings, B. D. Rainford, and H. J. Guggenheim, J. Phys. C: Solid State Phys. **3**, 307 (1970).

[51] F. M. Johnson and A. H. Nethercott, Phys. Rev. **114**, 705 (1959).

[52] S. M. Rezende, A. R. King, R. M. White, and J. P. Timbie, Phys. Rev. B **16**, 1126 (1977).

[53] R.W. Sanders, V. Jaccarino, and S.M. Rezende, Solid State Commun. **28**, 907 (1978).

[54] V. Jaccarino, A. R. King, M. Motokawa, T. Sakakibara, and M. Date, J. Mag. Mag. Mat. **31-34**, 1117 (1983).

[55] S. Saito, M. Miura, and K. Kurosawa, J. Phys. C: Solid State Phys. **13**, 1513 (1980).

[56] K. Kurosawa, M. Miura, and S. Saito, J. Phys. C: Solid State Phys. **13**, 1521 (1980).

[57] S. M. Rezende, R. L. Rodríguez-Suárez, and A. Azevedo, Phys. Rev. B **93**, 054412 (2016).

[58] I. Sänger, V. V. Pavlov, M. Bayer, and M. Fiebig, Phys. Rev. B **74**, 144401 (2006).

[59] Y. Shapira, S. Foner, and A. Misetich, Phys. Rev. Lett. **23**, 98 (1969).

[60] Y. Shapira and S. Foner, Phys. Rev. B **1**, 3083 (1970).

[61] K. W. Blazey, H. Rohrer, and R. Webster, Phys. Rev. B **4**, 2287 (1971).

[62] J. C. López Ortiz, G. A. Fonseca Guerra, F. L. A. Machado, and S. M. Rezende, Phys. Rev. B **90**, 054402 (2014).

[63] H. W. White and J. W. Battles, Solid State Commun. **8**, 313 (1970).

[64] D. L. Mills, Phys. Rev. Lett. **20**, 18 (1968).

[65] F. Keffer and H. Chow, Phys. Rev. Lett. **31**, 1061 (1973).

[66] F. Keffer and C. Kittel, Phys. Rev. **85**, 329 (1952).

[67] R. M. White, *Quantum Theory of Magnetism*, 3rd ed. (Springer-Verlag, Berlin,2007).

[68] S. M. Rezende and R. M. White, Phys. Rev. B **14**, 2939 (1976).

[69] A. B. Harris, D. Humar, B. I. Halperin, and P. C. Hohenberg, Phys. Rev. B **3**, 961 (1971).

[70] R. M. White, M. Sparks, and I. Ortenburger, Phys. Rev. **139**, A450 (1965).

[71] S. M. Rezende, J. Phys. C: Solid State Phys. **11**, L701 (1978).

[72] T. Oguchi, Phys. Rev. **117**, 117 (1960).

[73] S. M. Rezende, Phys. Rev. B **42**, 2589 (1990).